

XMM-Newton and Optical Observations of Cataclysmic Variables from SDSS

Eric J. Hilton, Paula Szkody, Anjum Mukadam

Astronomy Department, Box 351580, University of Washington, Seattle WA 98115

`hilton,szkody,anjum@astro.washington.edu`

Arne Henden, William Dillon

American Association of Variable Star Observers, 49 Bay State Rd., Cambridge, MA 02138

Gary D. Schmidt

Steward Observatory, University of Arizona, Tucson, AZ 85721

ABSTRACT

We report on *XMM-Newton* and optical results for 6 cataclysmic variables that were selected from Sloan Digital Sky Survey spectra because they showed strong HeII emission lines, indicative of being candidates for containing white dwarfs with strong magnetic fields. While high X-ray background rates prevented optimum results, we are able to confirm SDSSJ233325.92+152222.1 as an intermediate polar from its strong pulse signature at 21 min and its obscured hard X-ray spectrum. Ground-based circular polarization and photometric observations were also able to confirm SDSSJ142256.31-022108.1 as a polar with a period near 4 hr. Photometry of SDSSJ083751.00+383012.5 and SDSSJ093214.82+495054.7 solidifies the orbital period of the former as 3.18 hrs and confirms the latter as a high inclination system with deep eclipses.

Subject headings: novae, cataclysmic variables – stars: individual (SDSS J233325.92+152222.1, SDSS J093214.82+495054.7, SDSS083751.00+383012.5, SDSSJ 142256.31-022108.1, SDSS J154104.67+360252.9, SDSS J204827.91+005008.9) – X-rays: stars

1. Introduction

While the Sloan Digital Sky Survey (SDSS; York et al. 2000) reveals new cataclysmic variables (CVs) from its spectral database (Szkody et al. 2007 and prior references), the

correct identification of the type of close binary often requires follow-up observations utilizing time series and multiple wavelengths. Optical photometry, polarimetry, and spectroscopy can identify the orbital period, the spin period of the white dwarf and whether the object has a magnetic field. The X-ray light curve, flux and spectrum can distinguish a system with an accretion disk (dwarf nova or novalike) from those systems containing a white dwarf with a strong magnetic field (polar, which has the white dwarf spin synchronized to the orbit) or a lesser magnetic field (intermediate polar (IP) with a white dwarf spin shorter than the orbital period). For these magnetic systems in particular, the funneling of the accretion to the magnetic pole or poles creates a strong modulation of the X-ray fluxes (see Warner 1995 for a thorough review of the different types of CVs and their multi-wavelength light curves).

The high sensitivity and wide energy bandpass of *XMM-Newton* have shown this satellite to be ideal for measuring the X-ray fluxes and characterizing the X-ray source in the new CVs found in SDSS. The spin pulse and spectral temperature can be identified in systems with moderate accretion rates, while flares and softer spectral temperatures can be found in systems with extremely low accretion rates (Szkody et al. 2004b, Schmidt et al. 2005, Homer et al. 2005, 2006). In 2005-2006, we were granted *XMM-Newton* time to observe 6 CVs with strong HeII emission lines that were recently found from SDSS spectra as good candidates for containing magnetic white dwarfs. Unfortunately, except for SDSSJ233325.92+152222.2, the majority of the observations were conducted during times of high X-ray background, with the result that only portions of the total times on the sources could be used and only upper limits on the count rates could be obtained for the other 5 systems SDSS J083751.00+383012.5, SDSS J093214.82+495054.7, SDSSJ 154104.67+360252.9, SDSSJ 142256.31-022108.1 and SDSS J204827.91+005008.9. A request for re-observation was denied. We include here the results for all systems, together with some ground-based observations conducted along with X-ray observations that help elucidate the nature of several of the objects. For the rest of the paper, we will use abbreviations for the object names as SDSSJhhmm (hours and minutes of right ascension). Table 1 provides a summary of the properties of the 6 systems that were under study.

2. Observations and Data Reduction

2.1. X-ray

The two MOS detectors (Turner et al. 2001) and the EPIC pn detector (Striüder et al. 2001) on *XMM-Newton* were used to obtain X-ray observations of the 6 cataclysmic variables. In addition, the Optical Monitor (OM, Mason et al. 2001) obtained simultaneous optical observations, using the B filter (centered around 4500Å).. The pipeline products

were used to create light curves and determine B magnitudes. The data from the Reflection Grating Spectrograph were not useful due to low count rates. The details of the X-ray and OM observations, including dates, UT times, observation times (total time (TOT) and good time intervals (GTI) with background flaring times removed), and average count rates are listed in Table 2.

The data were reduced using the Science Analysis System (SAS) ¹, ver. 7.0.0 with calibration files current to August 15th, 2006. The data reduction followed the standard guidelines from the *XMM-Newton* Web site (VILSPA) and from the NASA/GSFC *XMM-Newton* Guest Observer Facility ABC Guide (ver. 2.01). The total observation data were used to identify the source visibility and background levels and then the data were screened to eliminate the high background where possible in order to increase the signal to noise. New event list files were created directly from the observation data files using the SAS tools. From these event list files, light curves were created in the 10-18 keV range using the entire chip for each detector and these files were used to identify and remove background flaring events. Each of the targets had different criteria for selecting good data intervals, depending on their individual light curves. For SDSSJ2333, SDSSJ2048 and SDSSJ1541, the high background count rates were most easily identified by using a count rate cut-off. For SDSSJ2333, data were ignored when the count rate exceeded 3.0 counts s⁻¹ for the pn and 0.6 counts s⁻¹ for both MOS detectors. For SDSSJ2048, we used limiting values of 12.0 counts s⁻¹ for the pn and 5.0 counts s⁻¹ for both MOS detectors as the background counts were higher throughout the observation. The limit used for SDSSJ1541 was 5 counts s⁻¹ for both pn and MOS detectors. For the other three targets, SDSSJ0837, SDSSJ0932 and SDSSJ1422, the background rate was stable throughout most of the observation, but increased significantly at either the beginning or the end of the observation. It was therefore easier to trim the data so that only data during the stable background times was used.

Five of our observations (SDSSJ0837, SDSSJ0932, SDSSJ1422, SDSSJ1541 and SDSSJ2048) had no obvious visible source. We note that in the case of SDSSJ1541, several bright pixels appear in the pn image somewhat near the expected location of the source. This is not apparent in the MOS, even though background sources that are fainter in the pn image than these bright pixels do appear in the MOS images. Additionally, the bright pixels do not show the psf of other sources visible in both detectors so we concluded that this was not the target. For these objects, we employed the following method to place an upper limit on the count rate. Using the pn detector images because of their increased sensitivity over the MOS, we used the target RA and Dec to place an aperture (360 pixel radius), and then

¹<http://xmm.esac.esa.int/sas/>

found the number of counts inside this target aperture, using an energy range of 0.1-15 keV. We then found the number of counts inside four circular background apertures of the same size, one in each quadrant. Each background aperture was a large area free of point sources located at a similar distance from the midplane of the detector. For our observations, the exposure time on the 12 pn chips varied slightly, so a count rate was determined for each aperture. We then calculated the count rate needed to have a 3σ detection, added this to the background, and compared to the count rate for the target aperture. In other words, given a measured background, we calculated the count rate needed to reach a given signal-to-noise, using:

$$\sigma = \frac{n\sqrt{t}}{\sqrt{n+b}} \quad (1)$$

where σ is the signal-to-noise, n is the count rate needed to reach that signal-to-noise, t is the time, and b is the background count rate. We used the average of the count rate needed for a 3σ detection in the four background apertures as our limit. As a consistency check, this analysis was carried out on a field source that appeared by eye to be very faint. The field source was a 5σ detection.

In order to ensure that real signal had not been removed when the flaring background sections were discarded, we also repeated this analysis keeping all of the exposure and limiting the energy range to 0.5-2.0 keV. In this analysis, no target was visible by eye in the image, and no target was above 3σ .

For the source that was successfully detected, SDSSJ2333, the event list files were filtered with the standard canned expressions, and were restricted to the well-calibrated regions of 0.2-15 keV for spectral analysis and 0.1-12.5 keV for light-curve analysis. With the pn detector, only single events (pattern = 0) were accepted for spectral analysis, and singles and doubles (pattern ≤ 4) for light-curve analysis. For the MOS detectors, quadruples and lower (pattern ≤ 12) were permitted for both the spectral analysis and the light-curve analysis. The data were binned to 20 counts per bin to increase the signal-to-noise ratio for the spectral analysis. The source region was taken to be a circular aperture with radius of 360 pixels for both detectors. The background region for the MOS detectors was determined from an annulus centered on the target and free of other sources while the pn background was determined using four rectangular regions, each on adjacent CCD chips, with similar Y locations as the target.

The resulting lightcurve is background-subtracted, and the times have been corrected

to the solar system barycenter using FTOOLS (Blackburn 1995)². The pn lightcurve data as well as the OM data were binned at 200 seconds to increase the signal-to-noise ratio.

SDSSJ0932 was the only other source to have sufficient counts in the OM to show variability on the orbital period. For this object, the OM data were binned at 60s to increase the S/N.

2.2. Ground-based data

Optical observations on SDSSJ0837, SDSSJ0932, SDSSJ1422 and SDSSJ2048 were conducted at the US Naval Observatory Flagstaff Station (NOFS), as well as at the George Observatory. The optical photometry summary can be found in Table 3.

For SDSSJ0932, the NOFS observations were made with the automated 1.3m wide-field telescope and a single 2048x4096 E2V back-illuminated CCD without any filter. This combination gives a pixel scale of 0.60arcsec/pix and a field of view of 20x40 arcmin. The exposure times were 90 seconds, with 50 seconds of dead-time between exposure. For the other NOFS targets, the 1.0m telescope and a SITe/Tektronix 102x1024 back-illuminated CCD without filter were used. This combination gives a pixel scale of 0.67arcsec/pix and a field of view of 11.3x11.3 arcmin. Exposure times averaging 200 seconds were used; deadtime at the 1.0m was always 40 seconds. In all cases, images were processed using standard techniques, and aperture photometry was performed using DAOPHOT (Stetson 1987) as implemented in IRAF. The exception was for SDSSJ2048, where the conditions were poor and DAOPHOT psf-fitting was used to obtain the highest signal/noise.

Once instrumental magnitudes were obtained, inhomogeneous ensemble photometry techniques following the guidelines of Honeycutt (1992) were used to obtain the final photometry. At least 10 stars in each field were used for the ensemble. Each error estimate is the quadrature sum of the Poisson and the ensemble errors.

All four optical targets have SDSS calibration photometry, but we also obtained B and V optical calibration at NOFS on photometric nights, using standards from Landolt (1983, 1992). The V-band calibration was used for the photometry shown in the figures and analysis, as the CCD response was closest to this passband. The calibration photometry is available on the AAVSO website³ and through their on-line comparison star database.

²tools available at <http://heasarc.gsfc.nasa.gov/lheasoft/ftools/>

³<http://www.aavso.org/>

The George Observatory measurements were made with a 0.46m telescope and SBIG CCD in cirrus sky conditions. The images were stacked in 5 minute bins and magnitudes were measured in comparison to other stars in the field to determine a differential light curve.

Circular polarization was also measured for SDSSJ1422 using the CCD Spectropolarimeter SPOL on the 2.3m Bok Telescope on Kitt Peak on the nights of 2005 March 16 and April 14. The instrument configuration and data acquisition was as described in Schmidt et al. (1992), with the exceptions of an improved quality camera lens and state-of-the-art 1200×800 pixel cosmetically perfect SiTE CCD with 2.2 e⁻ read noise that was thinned, back-illuminated, and anti-reflection coated by the University of Arizona’s Imaging Technology Laboratory.

3. Results

3.1. SDSSJ2333

This object was discovered and identified as a likely intermediate polar (Szkody et al. 2005; Sz05) from 9 hrs of photometry in 2004 that showed a 21 min period high amplitude modulation in its light curve, while an orbital period of 1.4 hrs was determined from a radial velocity curve obtained from 3.5 hrs of spectra. Southworth et al. (2007; Sw07) recently reported 4 hrs of photometry and spectroscopy covering 6 hrs over 2 nights in 2006. While their spectra confirmed and refined the period to 83.12 min, the photometry was consistent with a double-sinusoid variation indicating a spin period of 41.66 min and its harmonic at 21 min. This result implies two accreting poles causing the variation. The confirmation of an IP generally consists of a large amplitude variation at the spin period in X-ray, combined with a hard, absorbed X-ray spectrum. Fortunately, the best *XMM-Newton* data among the 6 objects were obtained for this source.

Figure 1 shows the light curve in both the optical OM (top panel) and X-ray pn (bottom panel). A prominent modulation is obvious in both light curves. The discrete Fourier transform (DFT) of these data, shown in Figure 2, reveals a period of 21 minutes (760 μ Hz), consistent with that found in the previous optical observations by Sz05. The period of 41.66 min (400 μ Hz) found by Sw07 is not evident. It is not clear if these differences are due to changes in the two accreting poles. The Sz05 optical dataset was obtained with a 1m telescope, using 140s integrations but was 9 hrs long (encompassing about 13 cycles if the period is 42 min). The Sw07 dataset was obtained with a larger (2.2m) telescope and 40s integrations but was only about 4 hrs long (somewhat less than 6 cycles of 42 min). Their unfolded light curve shows large variations in the depths of the minima so a few cycles could

influence the resulting pattern. Our XMM data are even shorter (about 3 hrs or only 4 cycles of 42 min) and the peaks and troughs are highly variable. Figure 3 shows the *XMM-Newton* data folded on the 41.66 min period. Due to the scatter, any difference in the two peaks in each cycle are not obvious.

We did fold the Sz05 optical dataset on 41.66 min and the resulting light curve shows two similar humps per cycle (Figure 4), unlike the light curve shown in Figure 4 of Sw07. The DFT of the Sz05 data (Figure 5) shows the orbital period (0.0002 Hz) and the prominent 21 min period but only a small insignificant peak that would be consistent with the 41.66 min period, in contrast to the Sw07 data which have a narrower and higher amplitude peak for the 42 min than the 21 min period. While the *XMM-Newton* data only show a 21 min period, the larger X-ray amplitude (2-3 times larger than the optical) confirms the IP nature of this source. Compared to the XMM results on the IP SDSS J1446+02, where the X-ray spin pulse maximum occurs 0.3 phase before the optical (Homer et al. 2006), the X-ray and optical pulses in SDSS J2333 appear to be in phase.

As further confirmation of the IP nature, we folded the data on the 41.66 min period using different energies (Figure 6 shows the resulting light curves). As is typical for IPs, the amplitude of the variability increases for lower energies, likely due to a local absorber in the system.

The pn spectrum of SDSSJ2333 is shown in Figures 7 and 8, binned at 20 counts per bin to increase the signal-to-noise ratio. The best fit XSPEC⁴ simple absorbed bremsstrahlung model gave a reduced $\chi^2 = 1.07$, with a hydrogen column density of the absorbing gas of $9.2 \times 10^{20} \text{ cm}^{-2}$ and a temperature of $5.1 \pm 1.4 \text{ keV}$ (Table 4). While this simple model provided a reasonable fit with a low reduced χ^2 , there was excess emission near 1 keV that could be due to a complex of Fe, Ne, O emission lines that is present in IPs (Mukai et al. 2003) and unresolved in our data. However, the fit with a mekal model (which includes emission lines) produced similar values (see Table 4) of temperature and column but does not fit the excess (Figure 7) either. While the spectrum is typical of IPs in showing a large absorption, the spectrum is not as hard as usual (10-20 keV), although it does not show a prominent soft X-ray component as evident in increasing numbers of IPs (Haberl et al. 2002; deMartino et al. 2006). We next tried partial covering absorbers (pcf) and cooling flow models (mkcflow). There was little improvement in the pcf model but the cooling flow seemed to fit the spectrum best (Table 4 and Figure 8). This type of model was used by Mukai et al. (2003) to fit the IP EX Hya.

⁴available at <http://heasarc.gsfc.nasa.gov/docs/xanadu/xspec/index.html>

3.2. SDSS J0837

Sz05 identified SDSSJ0837 as a polar candidate showing a cyclotron hump in the blue and TiO bands from the secondary star in the red. Follow-up polarimetry and spectroscopy (Schmidt et al. 2005) confirmed the polar nature, determined a spectral type of M5V, a distance of 330 pc and an orbital period of either 3.18 or 3.65 hr. Analysis of the spectrum showed this object has a very low accretion rate, similar to systems like MQ Dra (SDSSJ1553+5516) and SDSSJ1324+0320 (Szkody et al. 2003). *XMM-Newton* observations of these latter 2 systems (Szkody et al. 2004a) showed very low X-ray fluxes (10^{-14} ergs cm^{-2} s^{-1}) and luminosities ($<10^{29}$ ergs s^{-1}), and soft spectra (0.2-0.8 keV) characteristic of the secondary M star rather than a shock from accretion onto the white dwarf. While the high background rates combined with low source counts prevented a detection of SDSSJ0837 in our observations, the upper limit gives us a clue as to the nature of the X-ray flux. Table 5 compares the secondary spectral types, distance and pn count rates for the 3 sources. If the X-ray spectrum is similar to MQ Dra ($kT=0.8$ keV), then scaling by the distance squared predicts a count rate of 0.003 for SDSSJ0837, which is below the limit from our observation. The limit of 0.0042 for SDSSJ0837 would correspond to a 0.2-10 keV flux of $<8 \times 10^{-15}$ ergs cm^{-2} s^{-1} and an X-ray luminosity of $<10^{29}$ ergs s^{-1} . Thus, it appears that there is also no active X-ray shock in SDSSJ0837 and this system is indeed in the regime of extremely low accretion rate.

The count rate from the OM B filter gives a magnitude of 19.4, at the time of the X-ray observation, but there is no obvious variability in the OM light curve. Our optical photometry spans times a year prior to the X-ray data and 3 months after (Tables 2 and 3). Both data sets show the object at the same faint magnitude as evident in the SDSS photometry and that of Schmidt et al. (2005). Our light curves (Figure 9) show a repetitive structure (typical of polars) but with a low amplitude of modulation (as noted by Schmidt et al. and suggested to be due to a low inclination of the system). The spacing of the lowest points of the light curve are 3.14 ± 0.10 and 3.00 ± 0.10 hours for the 2 nights; Figure 9. Running a discrete Fourier transform on the data reveals periods of 2.98 ± 0.08 for Dec 15 and 3.06 ± 0.06 for Jan 27. Both of these methods show that the shorter period is the correct orbital period for this system.

3.3. SDSSJ0932

The SDSS spectrum of SDSSJ0932 is highly unusual (Szkody et al. 2006) with a very strong, asymmetric HeII 4686 emission line superposed on a blue continuum with only weak Balmer emission. Little information on this object exists in the literature, other than a dis-

covery spectrum by Munari et al. (1997) showing stronger Balmer emission and an abstract report (Holcomb et al. 1994) reporting weak ROSAT sources. The Center for Backyard Astrophysics web site contains a light curve made by Robert Fried⁵ that shows an eclipse and gives a period of 10.04 hrs, which is very long for a cataclysmic variable. Our *XMM-Newton* observation provided an upper limit of 0.014 c/s, confirming a low X-ray flux from this object, despite the strong HeII presence and its relatively bright optical mag ($g \sim 17.5$).

The OM data in the B filter show that an eclipse took place during the latter half of the pn observations (Figure 10). We also tried filtering the times of the pn data to exclude the eclipse, but still no source was visible. Our optical photometry obtained about 2 months prior to the X-ray observations is shown in Figure 11. A deep optical eclipse is evident which is offset to earlier phases from the center of an overlying hump. This offset appears different than the Fried light curve (where the eclipse appears centered in the hump structure), indicating a moving structure of the underlying emission region. The eclipse depth in B appears to be about 0.5 mag deeper than in V, as is typical for eclipses of a hot white dwarf and inner disk (Baptista, Steiner & Cieslinski 1994).

3.4. SDSSJ1422

This object was first identified in the Two-Degree Field (2dF) QSO survey (Croom et al. 2001) and suggested to contain a magnetic white dwarf by Marsh et al. (2002). The latter authors identified a possible 3.37 hr orbital period (with possible 1 cycle/day aliases) from spectroscopic data. This object also exists in the SDSS database (Szkody et al. 2004a) and shows similar spectra to those obtained by Marsh et al. The high X-ray background on this source resulted in very limited data so we were only able to place an upper limit on the X-ray flux. In addition, the source was too faint for any detection in the OM. However, our ground-based spectropolarimetry (Figure 12) obtained on two different nights (2005 March 16 for 960 sec and April 14 for 3600 sec) show coadded circular polarization values of +2.5% and +2.8% respectively, thus confirming this object as a polar. Polarization is present throughout the duration of the longer observation, which was obtained in three segments, and each segment displays a net circular polarization between +1.5% and +4%, with individual error bars of $\sim 0.5\%$. From the coadded results shown in Figure 10, it also can be seen that the polarization is approximately uniform over the optical spectrum, suggesting the smeared cyclotron harmonics of a high-temperature shock (characteristic of a bonafide

⁵<http://cbastro.org/results/highlights/uma6/>; note that this is a differential light curve that may not be calibrated with known standard stars

polar), as opposed to the isolated emission features of a low-accretion rate system. While the continuum flux level in 2005 looks similar to the SDSS spectrum from 2002, there is a rise at the blue end and the emission lines are not as strong, especially the HeII emission line. Thus, the accretion state may have been slightly different than in the earlier data.

While our optical photometry was obtained several years prior to the X-ray observations, we show the light curve in Figure 13 as there has not been any prior photometry published that we could find. There is a sinusoidal type modulation with full amplitude of ~ 0.4 mag on each night and pdm analysis gives a period of 4 hrs, but since this period is about the length of the data string on each night and the nights are too far apart to combine the data to obtain a better period, this value must remain as tentative. However, the photometry indicates the period could be longer than the estimate provided by Marsh et al. (2002).

3.5. SDSSJ2048

SDSSJ2048 is very similar to SDSSJ0837. Schmidt et al. (2005) provided the discovery information, identifying it as another very low accretion rate polar with an orbital period near 4.2 hr, an M3 secondary, and a distance of 260 pc. The *XMM-Newton* observations have a high background count over the whole chip, but the top half of the chip has systematically higher counts than the bottom half of the chip. Although we provide an upper limit, researchers should be cautioned that there may have been a problem with the pn detector during this observation. As with SDSSJ0837, there was no significant detection of the source, leading to a limit to the count rate of <0.013 . Using the same arguments as for SDSSJ0837 (Table 5), the expected count rate would be 0.005 c/s for a comparable spectrum as for MQ Dra. This is also consistent with our limit and argues for a lack of shock at the magnetic pole of the accreting white dwarf. The XMM limit would translate into a 0.2-10 keV flux of $<3 \times 10^{-14}$ ergs cm^{-2} s^{-1} and an X-ray luminosity of $<2 \times 10^{29}$ ergs s^{-1} .

The OM data show a very low count rate (Table 2) that translates into a B magnitude of 19.9. Our optical photometry obtained about 6 months prior to the X-ray observations appears to be about one magnitude brighter than the SDSS photometry but the observations were made in cirrus and the error bars are large. The light curve (Figure 14) shows variability of 0.3 mag which may be related to the orbital cycle but better photometry is needed to confirm this.

3.6. SDSSJ1541

This object was identified as a polar in Sz05. While the SDSS spectrum was obtained during a time of low accretion, the follow-up spectropolarimetry and photometry were obtained during high accretion states. During a high state, the X-ray flux is expected to be large and to show both soft and hard components. The OM data show the object at a low state, $B \sim 20$ mag. Unfortunately, the high radiation background during the *XMM-Newton* observation only left sufficient time to provide a limit of 0.0160 c/s. Combined with the unknown distance and spectrum, this value cannot constrain the source of emission.

4. Conclusions

Although high background rates prevented good observations of our faintest targets, the *XMM-Newton* pn observations have been able to confirm the IP nature of SDSSJ2333, and the limits on the fluxes of the very low accretion rate polars SDSSJ0837 and SDSSJ2048 show that these two systems have very low X-ray fluxes and luminosities ($< 10^{29}$ ergs s^{-1}) indicative of a lack of related accretion shocks. Our ground-based spectropolarimetry on SDSSJ1422 confirms it as a polar system and our OM and ground photometry on SDSSJ0932 provide good eclipses for this long period novalike system. While the presence of strong HeII emission was the initial defining characteristic of these 6 systems, the followup observations at other wavelengths have shown a wide variety of behavior.

This work was supported by *XMM-Newton* grants NNG05GL29GG and NNX06A38OG to the University of Washington and is based on observations obtained with *XMM-Newton*, an ESA science mission with instruments and contributions directly funded by ESA Member States and the USA (NASA). We thank the members of the AAVSO who contributed observations to determine the state of the systems close to the X-ray observations, especially Gary Walker. We also thank S. Levine for his help in making the NOFS 1.3m observations, and to the USNO for the use of their facilities.

REFERENCES

- Baptista, R., Steiner, J. E. & Cieslinski, D. 1994, ApJ, 443, 332
Croom, S. et al. 2001, MNRAS, 322, L29
deMartino, D. et al. 2006, A&A, 454, 287

- Haberl, F., Motch, C. & Zickgraf, F.-J. 2002, *A&A*, 387, 201
- Holcomb, S., Caillault, J. P. and Patterson, J. 1994, *BAAS*, 26, 1346
- Homer, L. et al. 2005, *ApJ*, 620, 929
- Homer, L. et al. 2006, *AJ*, 132, 2743
- Honeycutt, R. K. 1992, *PASP*, 104, 435
- Landolt, A. U. 1983, *AJ*, 88, 439
- Landolt, A. U. 1992, *AJ*, 104, 340
- Mason, K. O. et al. 2001, *A&A*, 365, L36
- Marsh, T. R. et al. 2002, *ASP Conf. Ser.* 261, 200
- Mukai, K., Kinkhabwala, A., Peterson, J. R., Kahn, S. M. & Paerels, F. B. S. 2003, *ApJ*, 586, 77
- Munari, U., Zwitter, T. and Bragaglia, A., 1997, *A&AS*, 122, 495
- Schmidt, G. D., Stockman, H. S. & Smith, P. S. 1992, *ApJ*, 398, L5
- Schmidt, G. D. et al. 2005, *ApJ*, 630, 1037
- Stetson, P. B. 1987, *PASP*, 99, 191
- Southworth, J., Gänsicke, B. T., Marsh, T. R., de Martino, D. & Aungwerojwit, A. 2007, *MNRAS*, 378, 635 (Sw07)
- Strüder, L. et al. 2001, *A&A*, 365, L18
- Szkody, P. et al. 2003, *ApJ*, 583, 902
- Szkody, P. et al. 2004a, *AJ*, 128, 1882
- Szkody, P. et al. 2004b, *AJ*, 128, 2443
- Szkody, P. et al. 2005, *AJ*, 129, 2386 (Sz05)
- Szkody, P. et al. 2006, *AJ*, 131, 973
- Warner, B. 1995, in *Cataclysmic Variable Stars*, CUP
- York, D. G. et al. 2000, *AJ*, 120, 1579

Table 1. Summary of Objects

Object	g mag	P_{orb} (hr)	Type	d(pc)	Ref ^a
SDSSJ0837	19.13	3.18	Polar	330	Sz05,Sch05
SDSSJ0932	17.45	10.0	NL	...	S06
SDSSJ1422	19.84	3.37 ^b	Polar	...	M02,S04
SDSSJ1541	19.70	1.4	Polar	...	S05
SDSSJ2048	19.38	4.2	Polar	260	Sch05,S06
SDSSJ2333	18.75	1.4	IP	...	S05

^aM02= Marsh et al. 2002; S04=Szkody et al. 2004;
 Sz05=Szkody et al. 2005; Sch05=Schmidt et al. 2005;
 S06=Szkody et al. 2006

^bM02 state this period could have 1 cycle/day aliases

Table 2. X-ray Observations

Target	Date	Instr	Filter	Time ^a (s)	UT Start	UT Stop	Ave Count rate ^b (C/s)	3 σ upper limit
SDSSJ2333	2006 Jun 04	pn	Thin1	10737/10436	09:00:47	11:59:44	0.184 \pm .005	
		MOS1	Thin1	12372/10866	08:38:28	12:04:40	0.078 \pm 0.003	
		MOS2	Thin1	12379/11271	08:38:28	12:04:47	0.074 \pm 0.003	
		OM	B	7200	09:55:16	12:03:42	1.3 \pm 0.4 (B=19.0)	
SDSSJ2048	2005 Apr 21	pn	Thin1	15829/7570	14:25:45	18:49:34		0.0138
		OM	B	16080			0.5 \pm 0.4 (B=19.9)	
SDSSJ0837	2005 Oct 07	pn	Thin1	12439/9700	09:38:52	13:06:11		0.0042
		OM	B	12961			0.8 \pm 0.3 (B=19.4)	
SDSSJ0932	2006 May 16	pn	Thin1	9581/8385	19:01:11	21:40:52		0.0148
		OM	B	10196			10.5 \pm 1.5 (B=16.71) ^c	
SDSSJ1541	2005 Aug 24	pn	Thin1	9628/4855	09:17:59	12:46:19		0.0160
		OM	B	10179			0.4 \pm 0.1 (B=20.0)	
SDSSJ1422	2006 Feb 07	pn	Thin1	5702/1996	21:08:43	23:33:03		0.0128

^apn,MOS times are Total time/Good Time Interval, OM times are from pipeline products

^bX-ray count rates determined from spectral reductions; OM count rates and B magnitude from pipeline products with error bar representing the variance

^cmagnitude is outside of eclipse

Table 3. Optical Photometry

Object	Obs	UT Date	Time
SDSSJ0837	USNO	2004 Dec 15	07:49-13:16
SDSSJ0837	USNO	2006 Jan 27	06:47-12:05
SDSSJ0932	USNO	2006 Feb 27	02:32-10:03
SDSSJ0932	George	2006 May 12	02:48-04:27
SDSSJ1422	USNO	2003 Jun 27	03:48-07:42
SDSSJ1422	USNO	2003 Jun 30	03:44-07:28
SDSSJ2048	USNO	2004 Sep 05	02:52-09:13

Table 4. Model Fits to SDSSJ2333

Model	Reduced χ^2	$N_H \times 10^{20} \text{ cm}^{-2}$	kT (keV)	Norm
bremss	1.07	9.2 ± 1.6	5.1 ± 1.4	2.2×10^{-4}
mekal	1.03	8.1 ± 1.6	5.2 ± 1.0	5.5×10^{-4}
pcf+mekal ^a	1.05	8.1 ± 1.6	4.9 ± 1.4	6.2×10^{-4}
mkcflow	0.81	8.8 ± 1.6	$0.4\text{-}17^b$	7.9×10^{-16}

^apcfabs fixed at 2×10^{23} ; resulting covering fraction of 13%

^blow and high temperatures of cooling flow

Table 5. Comparison of Low Accretion Rate Objects

Object	Sec	d (pc)	pn C/s
MQ Dra	M5	130	0.020
SDSSJ1324	M6	450	0.0012
SDSSJ0837	M5	330	<0.0042
SDSSJ2048	M3	260	<0.0138

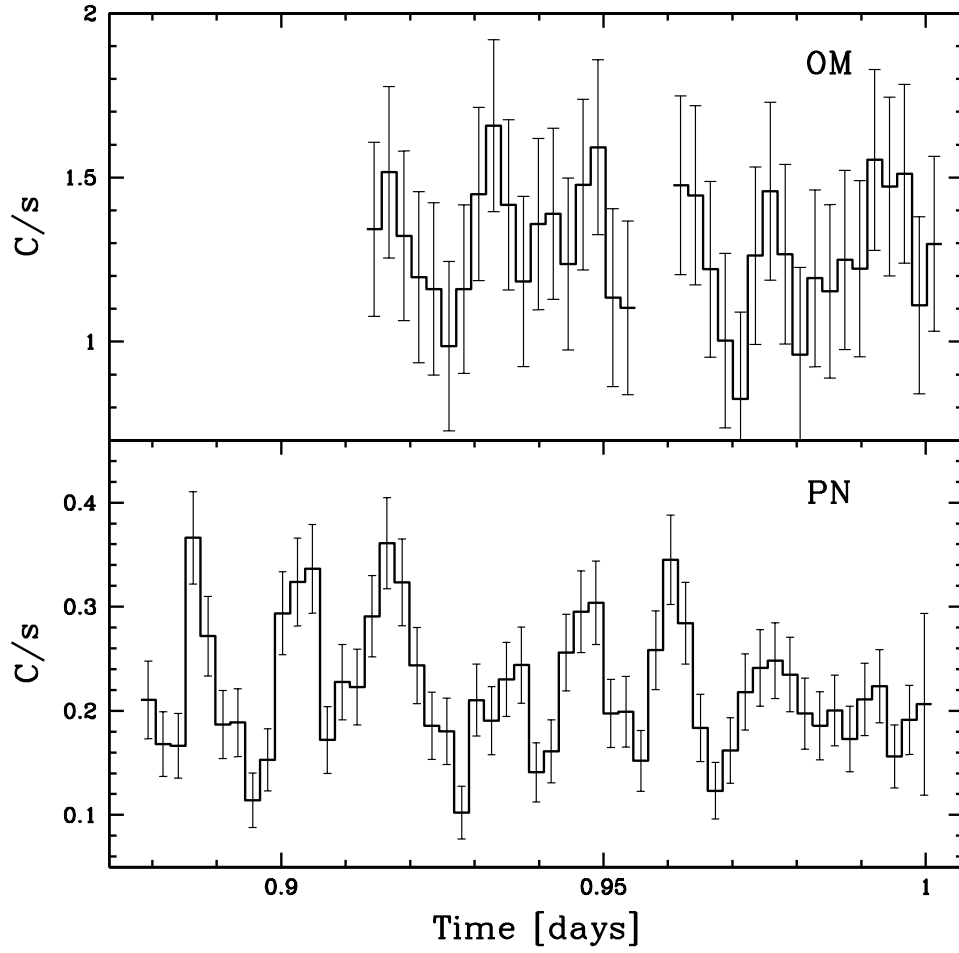


Fig. 1.— OM and pn light curves of SDSSJ2333 showing the strong modulation in both optical and especially X-ray.

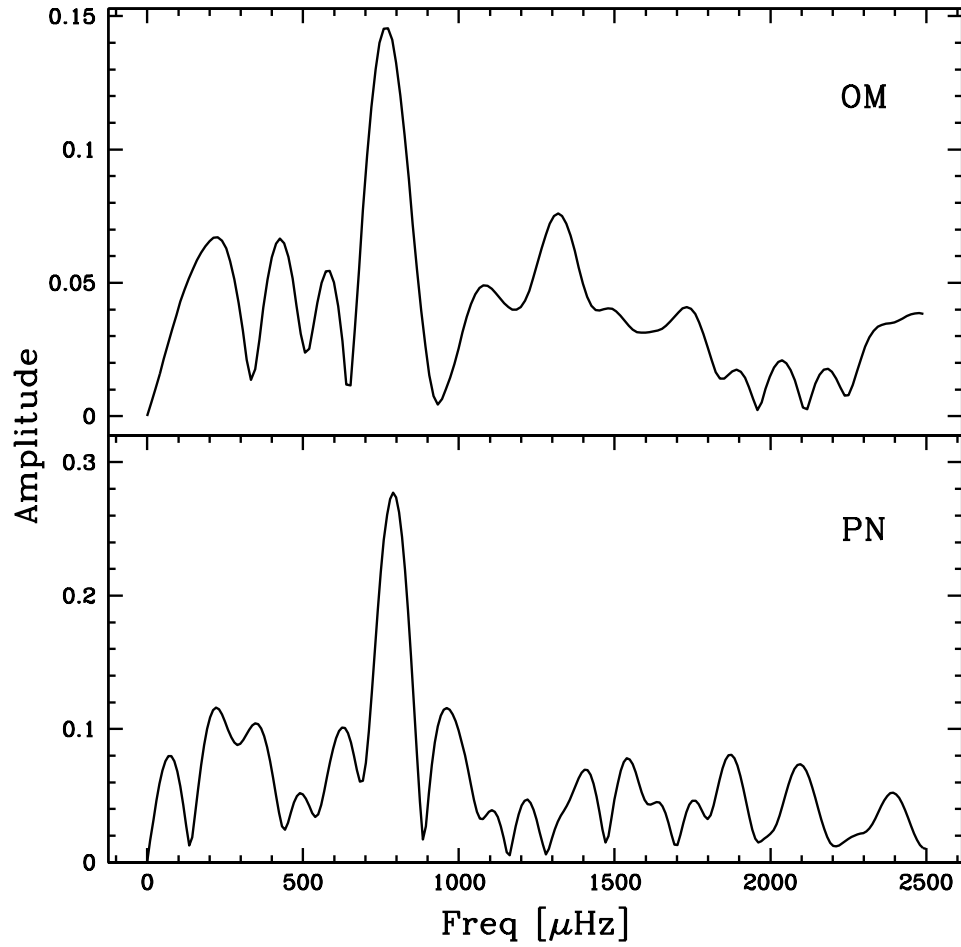


Fig. 2.— DFT of SDSSJ2333 showing the prominent period at 21 min and its large amplitude of modulation. Note there is no peak evident at the 41.66 min period ($400\mu\text{Hz}$) found by Southworth et al. (2007).

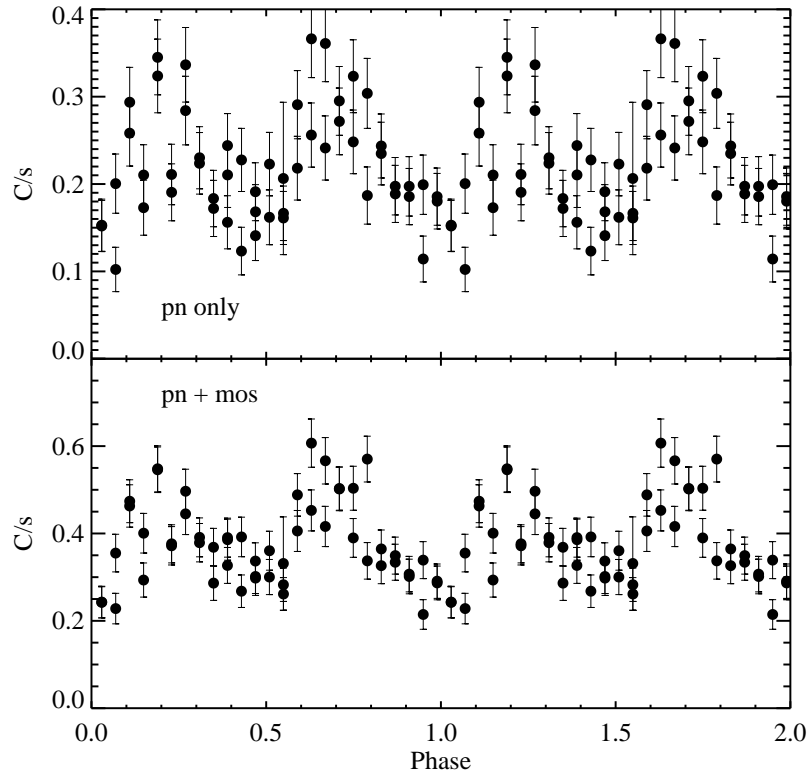


Fig. 3.— *XMM-Newton* pn and pn+mos data on SDSSJ2333 folded on the 41.66 min period.

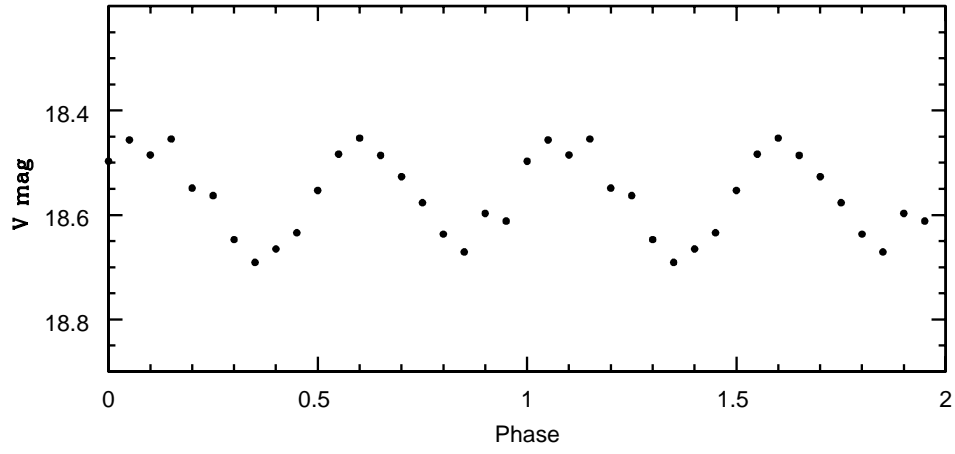


Fig. 4.— Optical data of SDSSJ2333 from Sz05 phased on the 41.66 min spin period.

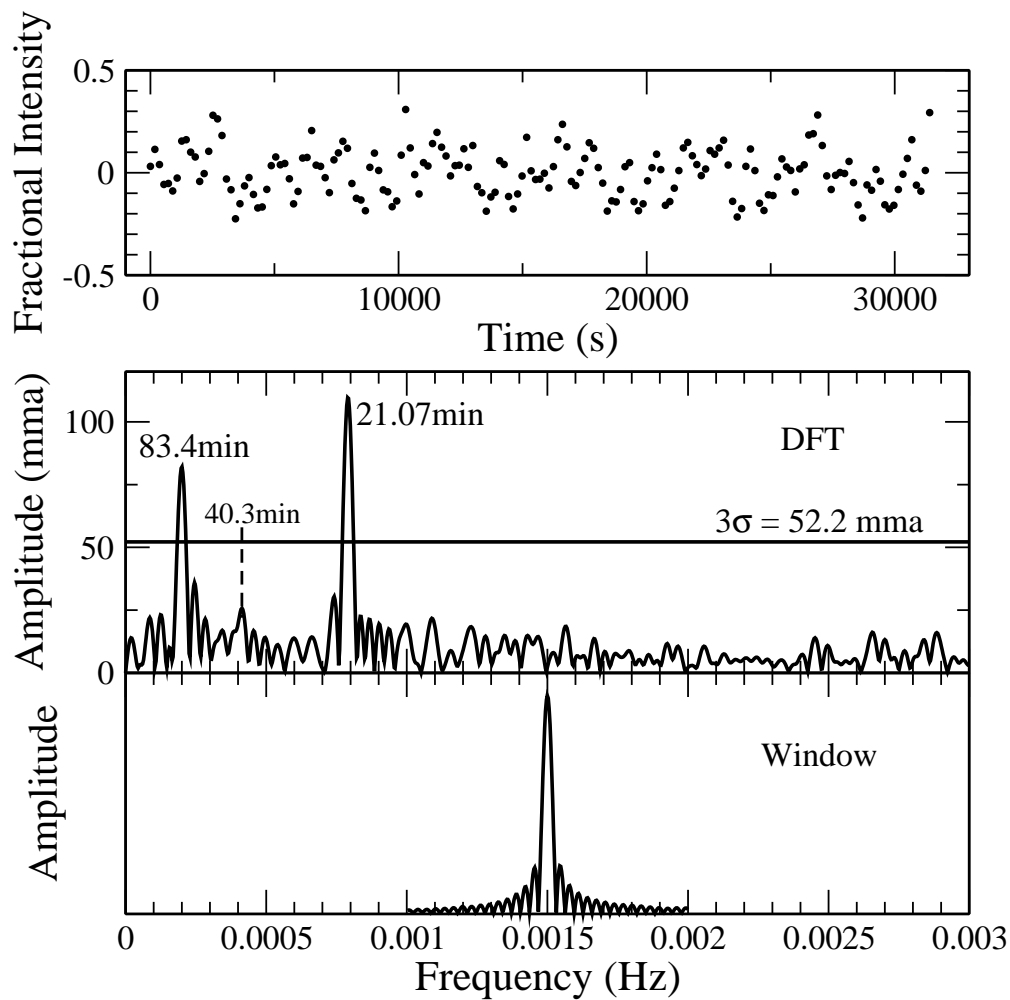


Fig. 5.— DFT of the optical data from Sz05. The 21 min period is evident but the 42 min period is not significantly detected above the noise. Amplitude units are milli modulation amplitudes. Top panel is the light curve divided by its mean (in intensity units) minus 1. Bottom panel is the transform of a noiseless frequency with the same time sampling as the data in order to show the alias pattern due to the finite length and gaps in the data.

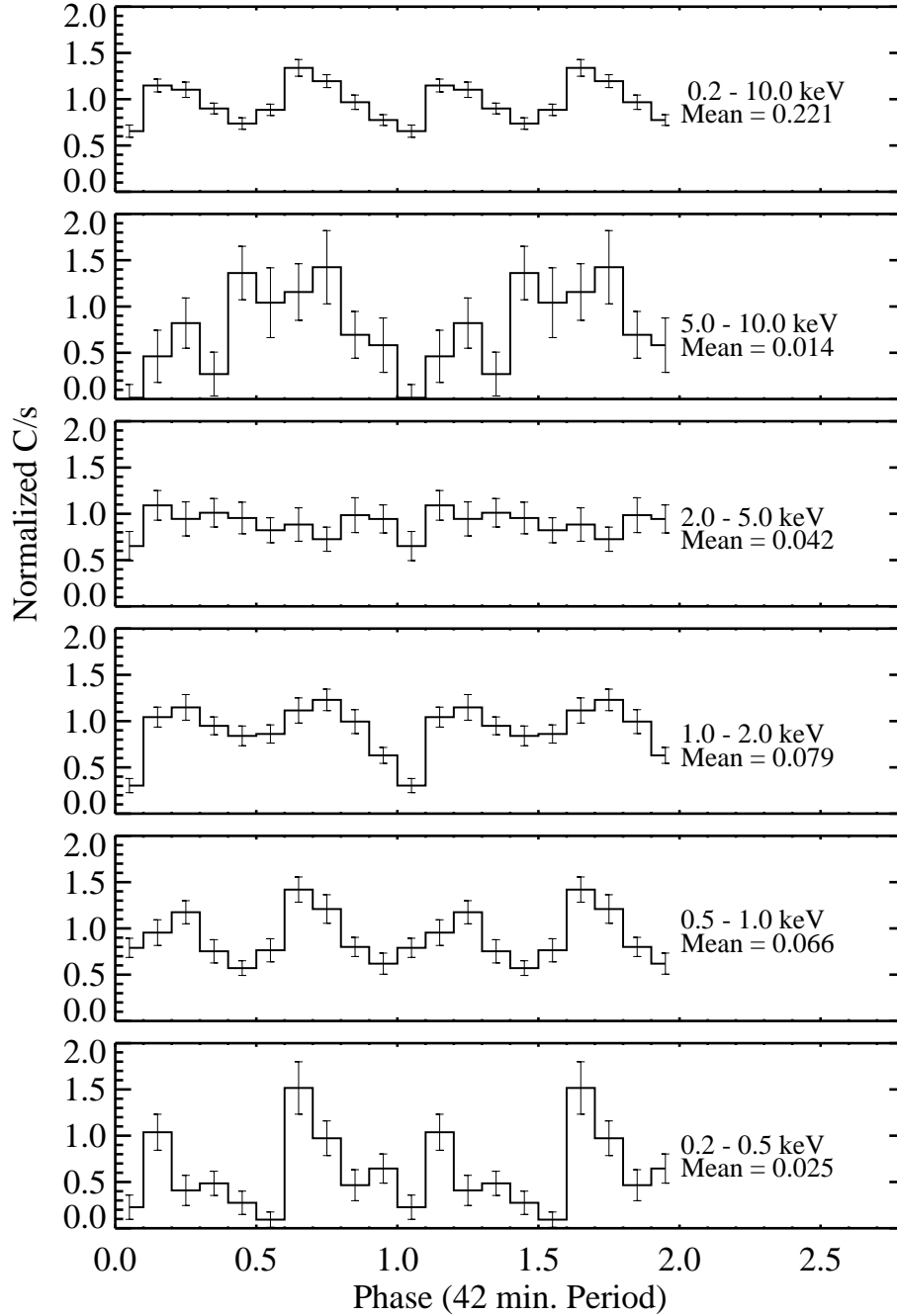


Fig. 6.— PN data of SDSSJ2333 at different energies and phased on the 41.66 min period.

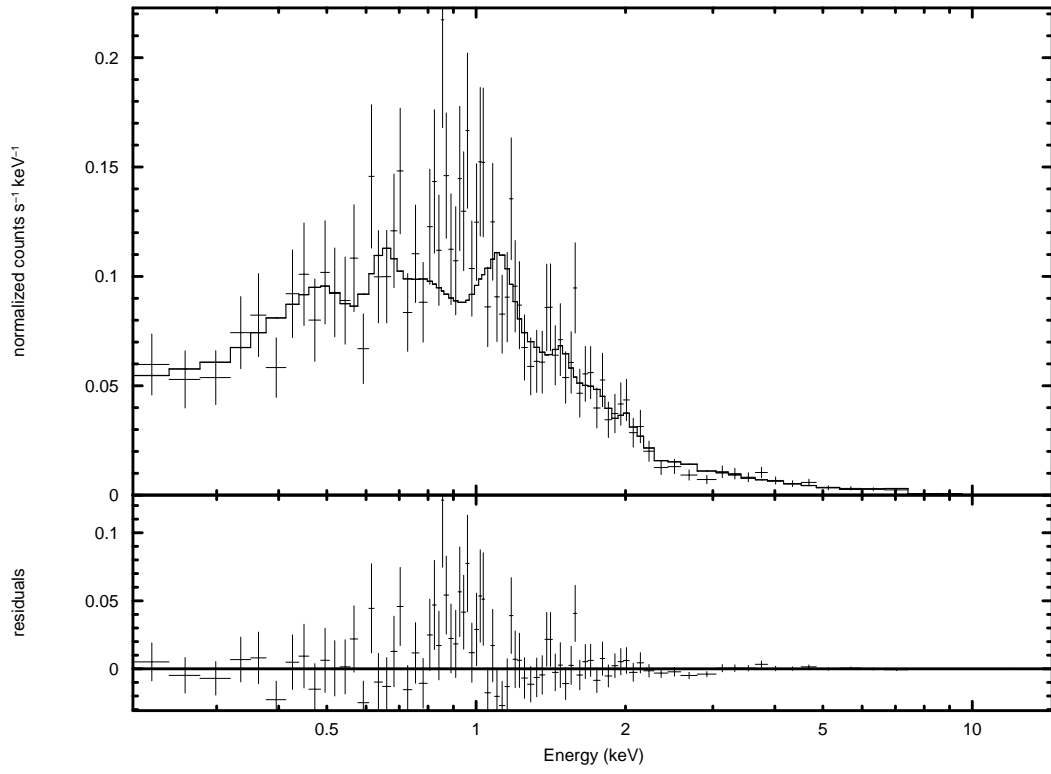


Fig. 7.— X-ray spectrum of SDSSJ2333 fit with a mekal model with $kT=5$ keV.

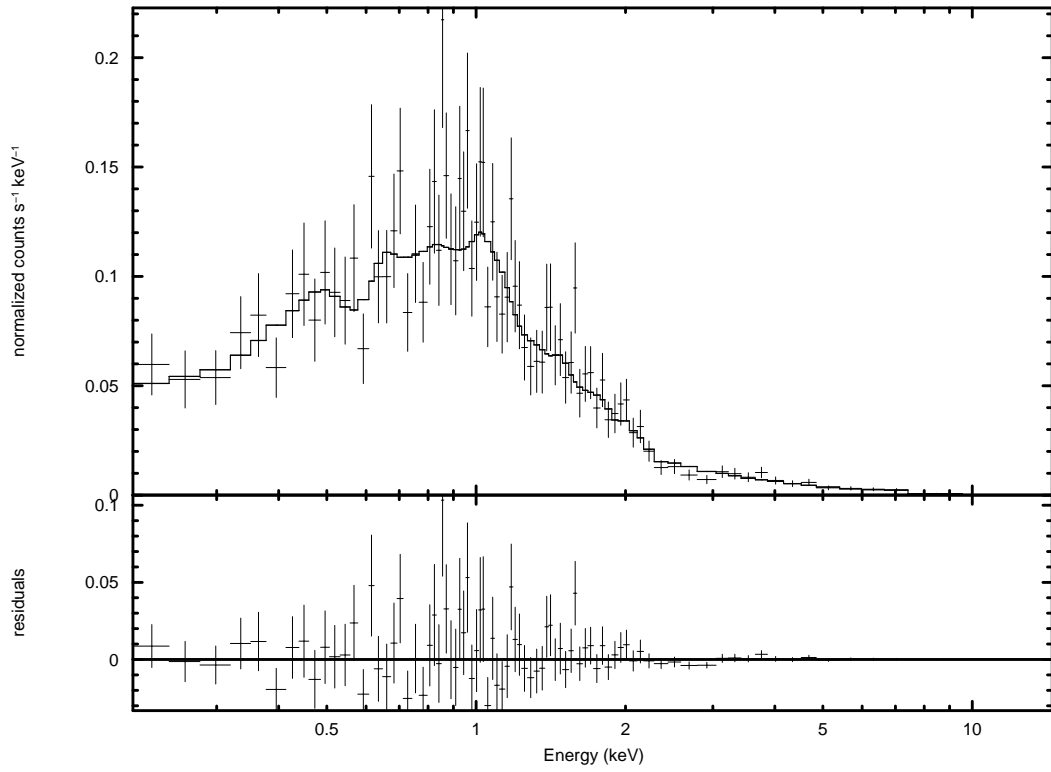


Fig. 8.— X-ray spectrum of SDSSJ2333 fit with a mkeflow model with kT from 0.4-17 keV.

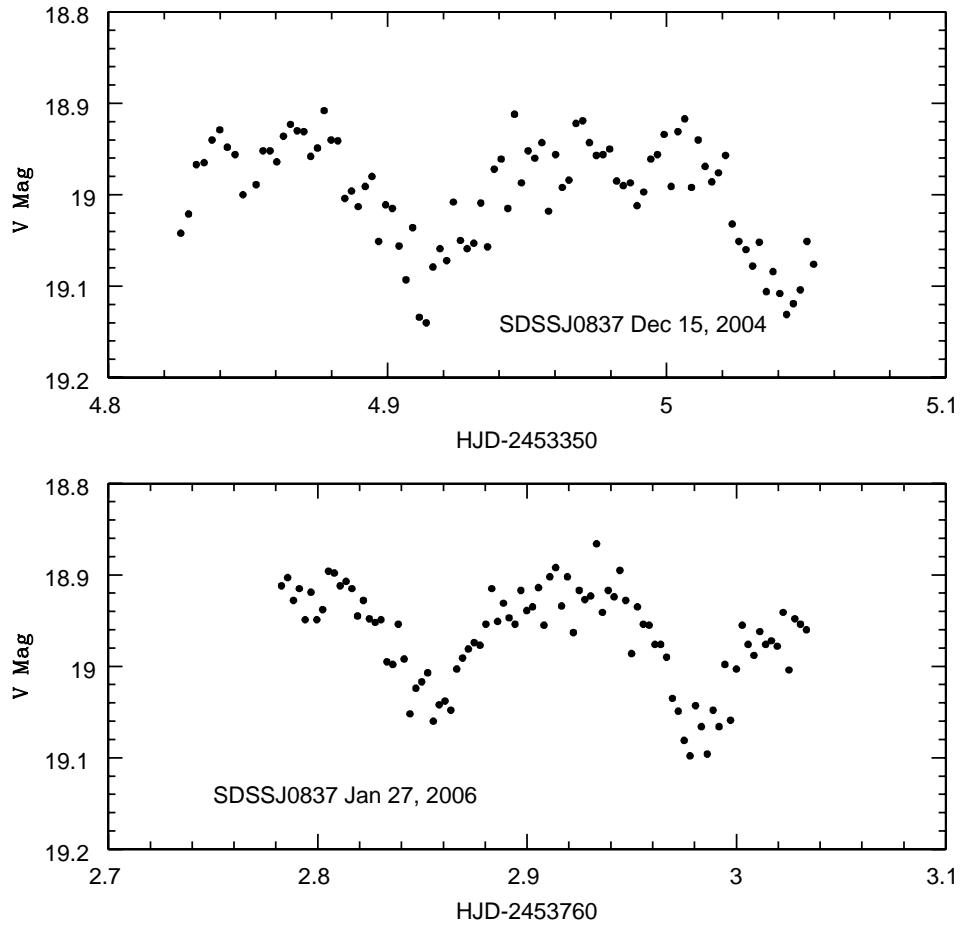


Fig. 9.— Ground-based data on SDSSJ0837. Error bars are 0.03 mag on Dec 15 and 0.02 mag on Jan 27.

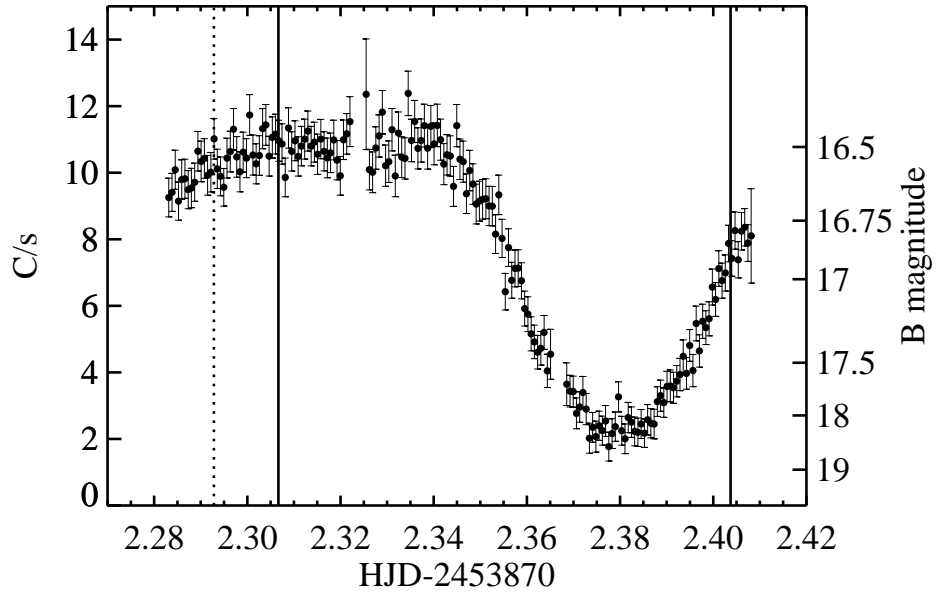


Fig. 10.— OM data on SDSSJ0932 in the B filter. Data are binned into 60 sec intervals. Dashed line is when the pn observation started; solid lines are the GTI intervals used for pn.

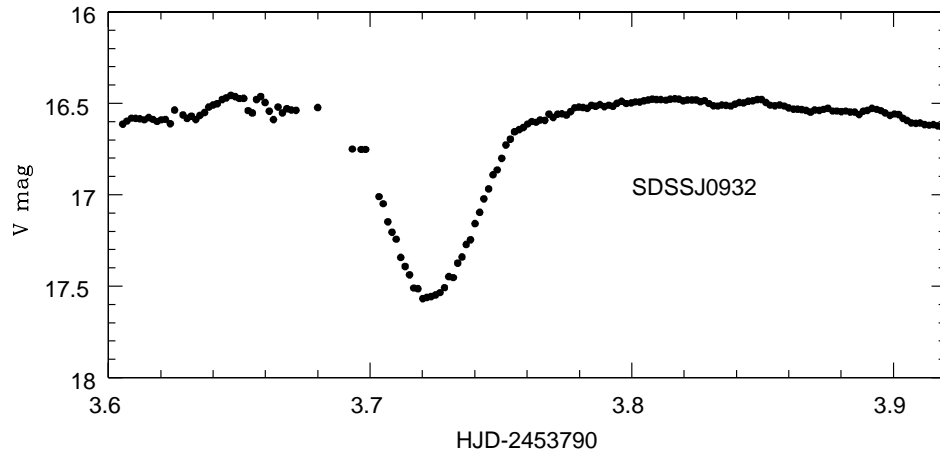


Fig. 11.— Ground-based data on SDSSJ0932 obtained 2006 February 27 UT. Error bars are 0.01 mag.

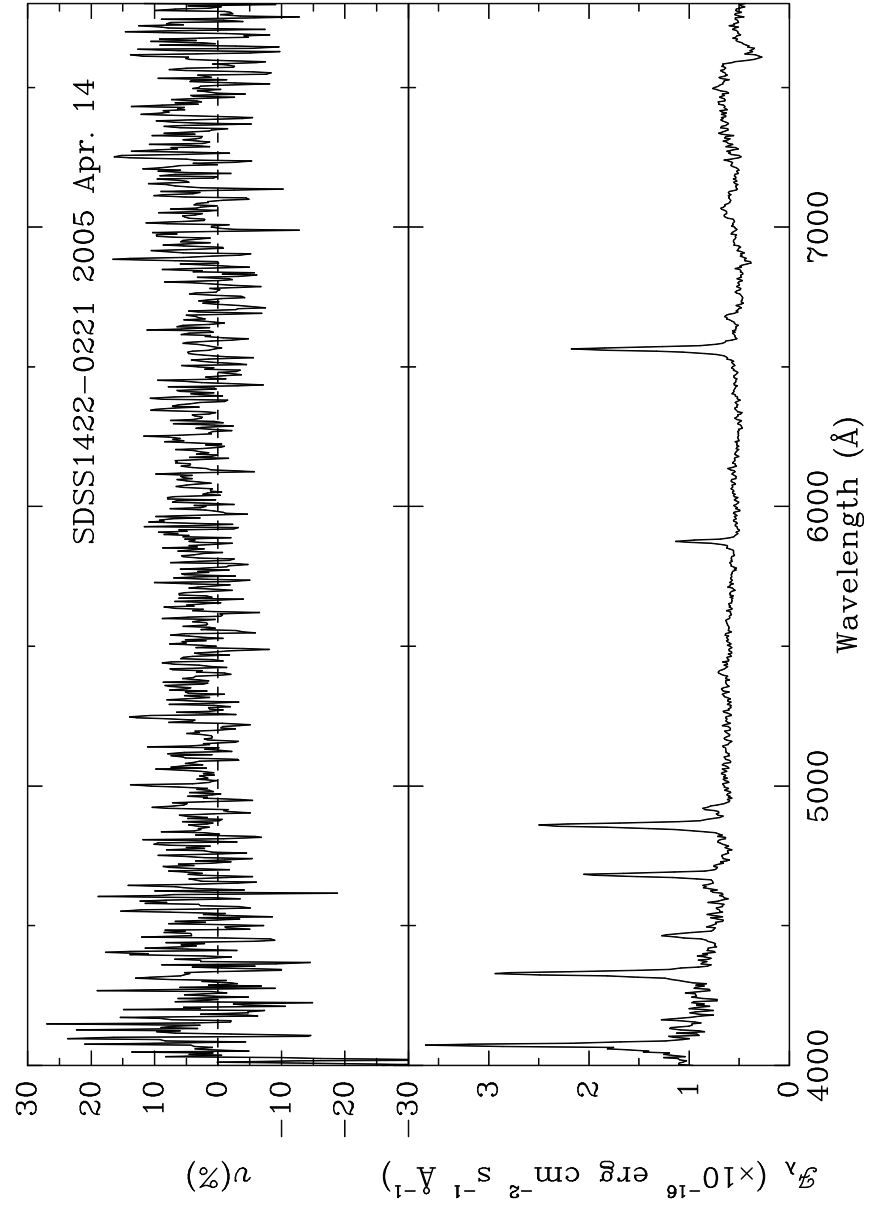


Fig. 12.— Circular polarization (top) and flux (bottom) spectrum of SDSSJ1422.

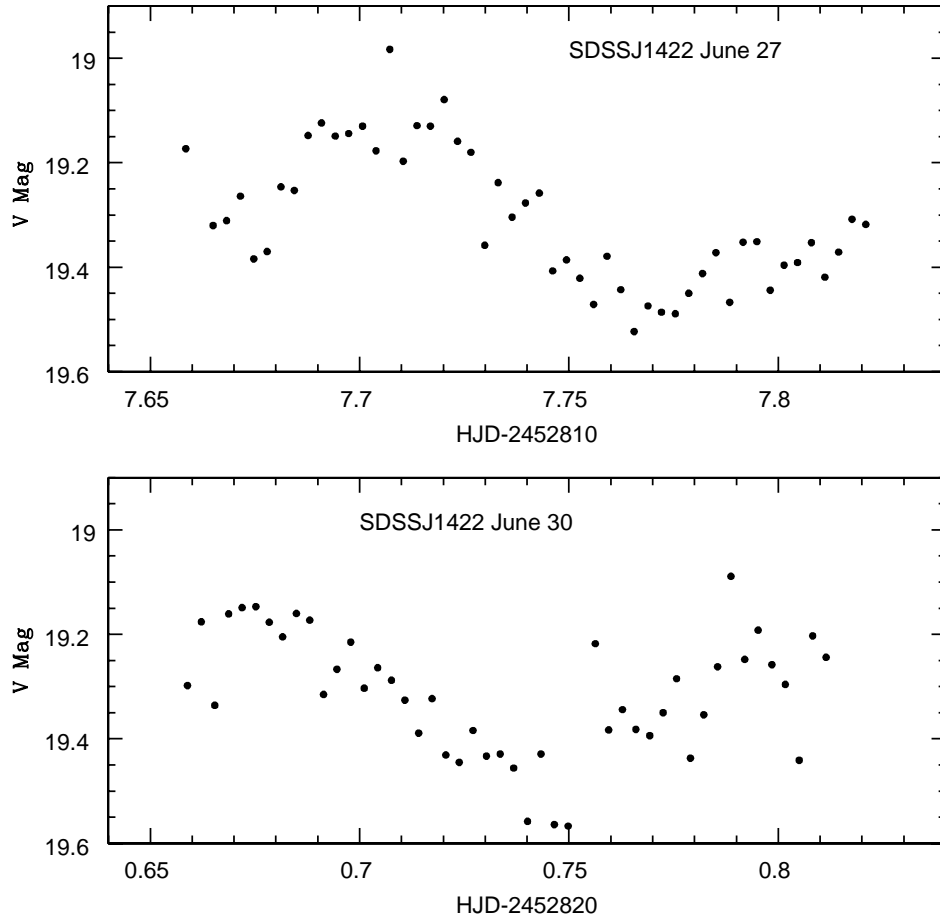


Fig. 13.— Ground-based data on SDSSJ1422. Error bars are 0.03-0.06 mag.

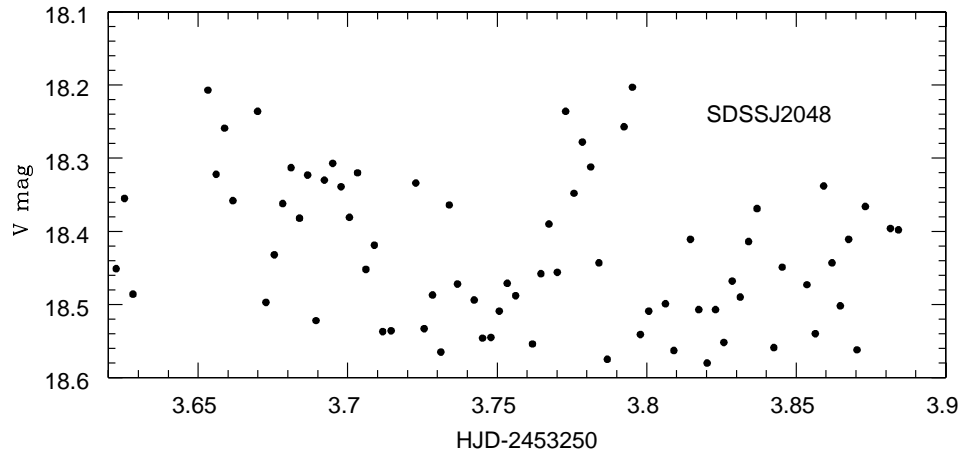


Fig. 14.— Ground-based data on SDSSJ2048 obtained in cirrus. Error bars are 0.05-0.14 mag.